Shoreline variability and coastal vulnerability: Mossel Bay, South Africa

Errol Wiles [a,b]*
Carlos Loureiro [c,d]
Hayley Cawthra[e,f]

a South African Institute for Aquatic Biodiversity, Makhanda, South Africa
b Institute for Coastal and Marine Research, Nelson Mandela University, Gqeberha, South Africa
c Geological Sciences, School of Agricultural, Earth and Environmental Sciences, University of KwaZulu-Natal, Durban, South Africa
d Biological and Environmental Sciences, Faculty of Natural Sciences, University of Stirling, Stirling, United Kingdom
e Geophysics and Remote Sensing Unit, Council for Geoscience, Cape Town, South Africa
f African Centre for Coastal Palaeoscience, Nelson Mandela University, Gqeberha, South Africa

* Corresponding author

Email: e.wiles@saiab.nrf.ac.za

Published in:

Estuarine, Coastal and Shelf Science
Volume 268, May 2022, #107789
Pages 1-13 DOI: 10.1016/j.ecss.2022.107789
URL: www.sciencedirect.com/science/article/abs/pii/S027277142200049X

Estuarine, Coastal and Shelf Science 268 (2022) 107789

Contents lists available at ScienceDirect

Estuarine, Coastal and Shelf Science

journal homepage: www.elsevier.com/locate/ecss

Shoreline variability and coastal vulnerability: Mossel Bay, South Africa

Errol Wiles [a,b,*], Carlos Loureiro [c,d], Hayley Cawthra [e,f]

[a] South African Institute for Aquatic Biodiversity, Makhanda, South Africa
[b] Institute for Coastal and Marine Research, Nelson Mandela University, Gqeberha, South Africa
[c] Geological Sciences, School of Agricultural, Earth and Environmental Sciences, University of KwaZulu-Natal, Westville Campus, Durban, 4000, South Africa
[d] Biological and Environmental Sciences, Faculty of Natural Sciences, University of Stirling, Stirling, FK9 4LA, United Kingdom
[e] Geophysics and Remote Sensing Unit, Council for Geoscience, Cape Town, South Africa
[f] African Centre for Coastal Palaeoscience, Nelson Mandela University, Gqeberha, South Africa

ABSTRACT

Highlights

- Landsat 7/8 and Sentinel 2A scenes capture variability in shoreline position
- DSAS-derived shoreline change rates indicate long-term stability
- Short-term shoreline change influenced by inlets, megacusps and rocky outcrops
- Alongshore variability in wave conditions reflected in shoreline change patterns
- Coastal processes and vulnerability described in three morphodynamic sub-cells

Shoreline variability and coastal vulnerability: Mossel Bay, South Africa.

Errol Wiles[a*, b], Carlos Loureiro[c, d] & Hayley Cawthra [e, f]

[a] South African Institute for Aquatic Biodiversity, Makhanda, South Africa;

[b] Institute for Coastal and Marine Research, Nelson Mandela University, Gqeberha, South Africa

[c] Geological Sciences, School of Agricultural, Earth and Environmental Sciences, University of KwaZulu-Natal, Westville Campus, Durban 4000, South Africa

[d] Biological and Environmental Sciences, Faculty of Natural Sciences, University of Stirling, Stirling FK9 4LA, United Kingdom

[e] Geophysics and Remote Sensing Unit, Council for Geoscience, Cape Town, South Africa

[f] African Centre for Coastal Palaeoscience, Nelson Mandela University, Gqeberha, South Africa

*Corresponding Author: e.wiles@saiab.nrf.ac.za

Abstract

Coastal erosion may cause significant damage to property and infrastructure with far reaching socio-economic consequences. Assessing the site-specific shoreline dynamics is fundamental to understand the morphodynamic behaviour of a particular coastal area, as well as the associated coastal hazards. However, changes in shoreline position, even when significant, are not necessarily associated with increased coastal hazards. In this contribution we investigate the impact of short-term changes in shoreline position within a crenulated embayment of Mossel Bay. The 30 km-long embayment, located in the Western Cape region of South Africa, lies in a high-energy wave-dominated, micro-tidal setting. Mossel Bay is heavily populated and experiences an influx of tourists year-round. Much of the coastal community and infrastructure lies within 25 – 40 m of the foredune toe.

Georeferenced Landsat 7/8 and Sentinel 2A scenes are used to manually digitise shoreline position in ArcMap, using the "wet/dry" line as a shoreline position proxy. The Digital Shoreline Analysis System was then used to generate shoreline change statistical metrics. Wave conditions were modelled using SWAN wave model, implemented using a nested grid approach with a high-resolution (10 m) inshore

29 grid, and a lower resolution (50 m) offshore regional grid. The nearshore wave field during mean and
30 storm conditions was obtained along the 15 m isobaths along the entire embayment.
31 The embayment's orientation in relation to the prevailing swell direction results in significant
32 alongshore variability in nearshore wave conditions; wave heights increase towards the east along the
33 embayment. This variability in wave forcing is reflected by the changes in shoreline position in both
34 long and short-term, computed using the end-point rate method. However, the areas of higher shoreline
35 change are not those experiencing the worst detrimental effects.
36 Over the long-term, the present-day Mossel Bay embayment is relatively stable, with no significant
37 signs of extensive accretion or erosion. However, rapid migration the shoreline is documented on a
38 seasonal scale (short-term) with significant change proximal to river mouths, areas influenced by
39 megacusps, and regions where the highly dynamic shoreline behaviour is constrained by rocky
40 platforms and unable to freely adjust to variations in forcing. Thus, Mossel Bay is divided into three
41 sub-cells in terms of coastal processes and coastal vulnerability with hazards associated with the
42 location of such infrastructure rather than the specific patterns of shoreline change.
43

44 **1. Introduction**

45 Located at the interface between marine and terrestrial settings coastal zones are complex systems, yet
46 understanding their dynamics is fundamental to sustainable coastal zone management. Coastal and
47 shoreline change occurs over diverse temporal and spatial scales as a result of morphodynamic
48 interaction between the coastal sediments, geology and geomorphology, wave and wind climate, tidal
49 and ocean currents, anthropic influences and infrastructures (Carter and Woodroffe, 1994; Del Rio and
50 Benavente, 2013; Hapke et al., 2016). Understanding coastal change is a challenging task with multiple
51 influential factors exerting non-linear and often site-specific influences (Cooper et al., 2004). In
52 exposed, wave-dominated environments, coastal change is primarily driven by variation in wave
53 conditions, but nearshore waves are significantly controlled by the geomorphology of the coast and the
54 bathymetry of the shoreface and continental shelf, affecting the patterns of sediment transport, erosion
55 and deposition (McNinch, 2004). In any given coastal location, the bathymetry itself is determined by
56 the availability and distribution of shoreface sediments and the geological sub/outcrops relative to mean

sea level. Hence, the geological framework exerts a significant control in unconsolidated shoreface dynamics and coastal processes in response to wave climate (Thieler et al., 1995; McNinch, 2004; Del Rio and Benavente, 2013; Cooper et al., 2018).

The product of these interactions is the shoreline position; an important geoindicator for sandy coastal environments (Carapuço et al., 2016; Cawthra et al., 2020) that changes its shape and position over multiple spatial and temporal scales (Burningham and Fernandez-Nunez, 2020). Although there are a multitude of coastal features that may be used to define the shoreline position, from the wet-dry line to the vegetation line (Boak and Turner, 2005), the relative seaward or landward migration of the shoreline reflects the alongshore and cross-shore variability in coastal processes which force the addition or loss of material from the coast. Thus, variation in shoreline position marks the logical starting point when assessing coastal change as it provides a reference framework against which other influences may be compared, and coastal dynamics better understood.

Sandy beaches, extending from the nearshore zone to the foredune, represent one of the most dynamic and responsive sedimentary and morphological environments on Earth (Jackson and Short, 2020). Phases of accretion and erosion are natural, often associated with periods of high and low relative wave energy and/or changes in wave direction (Harley et al., 2015). Alternation between phases are typically linked to seasonal cycles; erosional phases in winter, and accretional phases during summer, (Senechal et al., 2015; Velegrakis et al., 2016; Umeda et al., 2018). However, variability in beach morphology can be considered at a range of timescales (Senechal and Alegria-Arzaburu, 2020), particularly short-term or event-based change driven by extreme single storms or storm groups (Ferreira, 2005), or at the timescale of years and decades, often linked to climate variability or changes in sediment supply (Smith et al. 2014; Senechal and Alegria-Arzaburu, 2020). Geologically-controlled sandy beaches add further complexity to seasonal sediment transport and deposition by introducing hard, non-erodible surfaces that limit the variability of unconsolidated beach profiles (Larson and Kraus, 2000; Vousdoukas et al., 2007; Gallop et al., 2020) while altering nearshore hydrodynamics (Cleary et al., 1996; Larson and Kraus, 2000; Vousdoukas et al., 2007; Storlazzi et al., 2010; Velegrakis et al., 2016), increasing erosion rates through scouring and reduced water infiltration (Walton and Sensabough, 1979; Larson and Kraus, 2000; Vousdoukas et al., 2009) and potentially limiting cross and along-shore sediment transport

(Vousdoukas et al., 2007; Gallop et al., 2020). In naturally functioning systems, undisturbed by anthropogenic interference and where direct human pressure is low to non-existent, phases of accretion and erosion and associated shoreline change pose no immediate risk as the coastal system is naturally dynamic. However, when infrastructure is placed within the beach or immediately landward, the interaction of a naturally dynamic system with human occupation and uses can have far-reaching consequences (Thom, 2020), including: loss of property, infrastructure, public access and amenity value (Brew et al., 2011). Hence, understanding the dynamics of the coastal zone and the impact on coastal erosion, as well as the implications for coastal hazards and associated risks to human occupation is a long-lived concern for coastal managers (Philips and Jones, 2006). Increased coastal erosion can also increase risk associated with potential loss of economically valuable land/infrastructure, sense of place and ecological services (Alexandrakis et al., 2015).

Assessing coastal vulnerability through various means is a necessary next step in management practice, highlighting areas of most concern and allowing coastal management focus to be directed effectively and efficiently. Typically, coastal vulnerability assessments fall into one of four categories: index-based methods, indicator-based approach, GIS-based decision support systems, and methods based on dynamic computer models (ETC CCA, 2011). While each particular approach is meaningful, adding value to policy and management, integrated approaches yield more comprehensive results to analyse and interrogate, thus allowing more robust evaluation of vulnerability at complementary spatial and temporal scales (McLaughlin and Cooper, 2010).

The embayment of Mossel Bay, located in the Western Cape, is heavily populated with significant infrastructure located within a densely vegetated primary coastal dune, in places less than 10 m from the high-water line. In Mossel Bay, as in many locations worldwide, there is significant potential for interaction between the natural beach system and coastal infrastructure. It is this interaction, and the associated coastal hazards that are the focus of this research. The aim of this paper is to analyse shoreline change in Mossel Bay at different time-scales and evaluate its relation to coastal hazards and vulnerability. To achieve this, we investigate: 1) long and short-term shoreline change using satellite imagery, 2) alongshore variability in the wave conditions, 3) presence and characteristics of erosional

hotspots and, finally, 4) the evolution of the shoreline and forcing in the context of coastal hazards and coastal development along Mossel Bay.

2. Regional setting

South Africa's Cape South Coast (hereafter: South Coast) extends semi-continuously from Cape Hangklip in the west to Plettenberg Bay in the east (Fig. 1a) and is characterised by a seaward-dipping, low-relief coastal plain incising the base of the Cape Fold Belt. Extension, deformation associated with the Gondwana break-up (Watkeys, 2006), led to the formation of a series of rift basins along the southern margin of Africa that are characterised by graben and half-graben structural styles and infilled with Mesozoic sedimentary deposits (McMillan *et al*. 1997; Broad *et al*. 2006, 2012; Paton *et al*. 2006). The South Coast has served as a significant sediment sink, particularly with respect to the deposition and accumulation of marine, aeolian and lacustrine sediment during the Neogene and Quaternary Periods (Dingle et al. 1983, Flemming and Martin, 2017). The continuity of this coastline is fragmented into a series of variable sized coastal embayments that correspond morphologically to log-spiral embayed beaches. Offshore, the Agulhas Bank has been extensively planed by sea-level fluctuations in Neogene and, in particular, Pleistocene times (cf. Cleghorn, et al., 2020). Inshore, more recent deposits are preserved as low-relief ridges, shoals and shelf sands along the now submerged course of the Great Brak River (Cawthra et al., 2015). Onshore, upper Cenozoic shallow marine deposits of the Klein Brak Formation and aeolian sediments of the Waenhuiskrans Formation belong to the Bredasdorp Group and overlie older Neogene Wankoe Formation deposits in places (Malan, 1990). The younger unconsolidated Strandveld Formation constitutes the modern beaches and dunes. Palaeo shorelines have been extensively investigated in this bay (e.g., Carr et al., 2010; Jacobs et al., 2011; Roberts et al., 2012; Cawthra et al., 2015; 2018) as the Mossel Bay coastline was always a valuable resource to humans (Marean et al., 2007; Marean et al., 2015).

Regarding the wider oceanographic and climatic setting, the southwestward-flowing Agulhas Current closely follows the continental shelf break southward along South Africa's east coast and the Agulhas Falkland Fracture Zone moving offshore south of Port Elizabeth (350 km east of Mossel Bay) where the Agulhas Bank shelf broadens from ca. 50 km to ca 130 km (Martin and Flemming, 1986). The offset in continental shelf and interaction with the Agulhas Current results in an eastward-flowing Agulhas

140 counter current and localised eddies (Rogers, 1971). Thus, Mossel Bay is not directly influenced by the
141 Agulhas Current core, but rather a dynamic eddy and counter-current system. The South Coast receives
142 precipitation derived from westerly driven frontal systems that bring winter rainfall and the Intertropical
143 Convergence Zone bringing summer rain from the east, resulting in a year-round rainfall regime (South
144 African Weather Bureau 1986; Taljaard 1996). Spring and autumn rainfall, associated with coastal cut-
145 off low-pressure systems, may result in flooding in the region (Taljaard 1996).
146 The Mossel Bay embayment represents a micro-tidal coastline, with spring tides exhibiting a vertical
147 range of less than 2 m (Davies, 1980; South African Navy, 2017). The spring tidal range for much of
148 the coastline lies between 1.8 and 2.0 m with neap tidal ranges between 0.6 and 0.8 m (Cooper, 2001).
149 The coastline is swell dominated with prevailing wave direction originating from the southwest,
150 resulting in a net eastward longshore drift, with average conditions characterised by a significant wave
151 height of 2.7 m and mean wave period of 6.6 s, while storm conditions (95% exceedance) are associated
152 to significant wave heights of 4.6 m and mean wave periods of 8.1 s. The rate of contemporary sea-
153 level rise along the southern Cape coast is estimated at 1.57 mm/year (Mather et al., 2009).

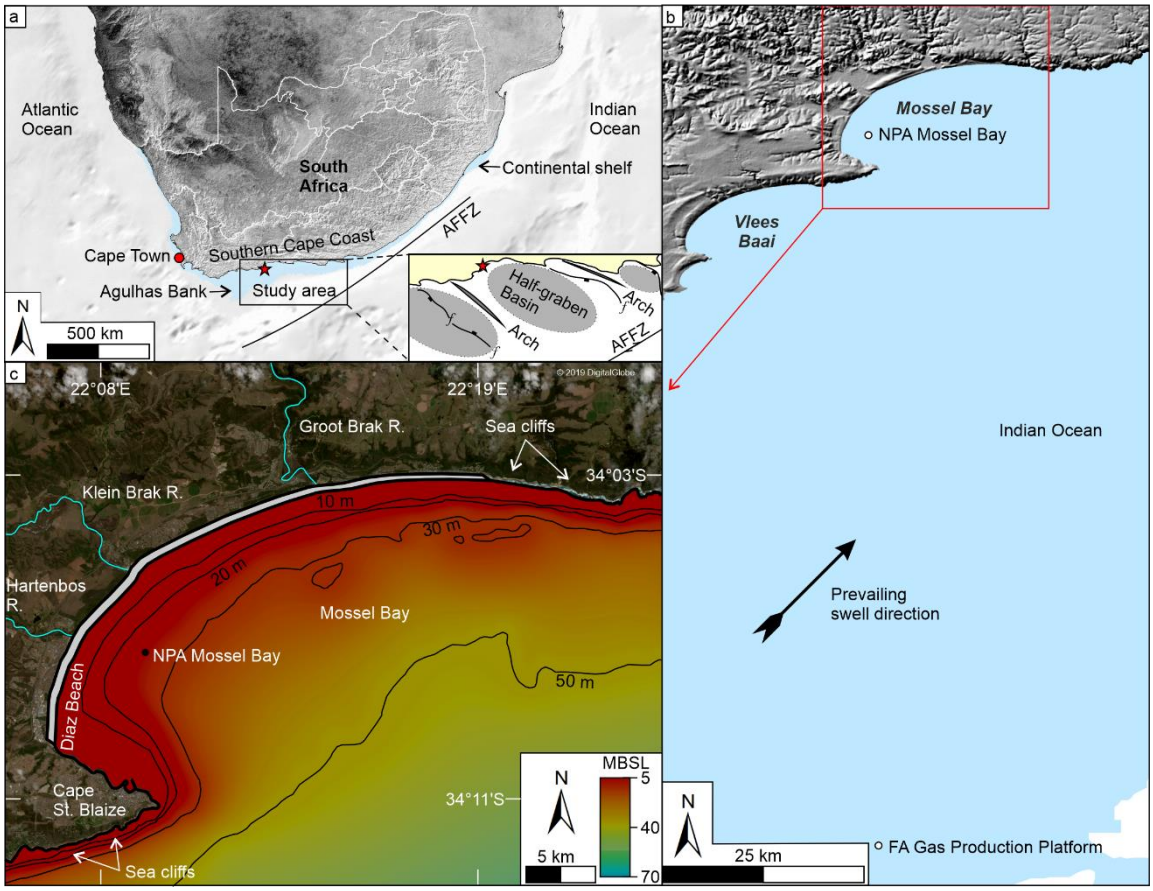

154 Fig. 1. a) Southern Africa; the Agulhas Bank hosts several structural basins (inset) bound offshore by
155 the Agulhas Falkland Fracture Zone (AFFZ). Note: location of the study area (red star) mid-way along
156 the southern Cape coast. b) Mossel Bay is a log-spiral bay in the Western Cape, South Africa. The
157 Transnet National Port Authority (NPA) wave buoy lies within Mossel Bay, while the FA Gas
158 Production Platform wave buoy is located directly south of the embayment. c) General bathymetry of
159 Mossel Bay as digitised from South African Navy (SAN) Chart 123. (Base map from Google Earth, ©
160 2018 AfriGIS (Pty) Ltd; © 2019 DigitalGlobe).

161

162 **3. Data and Methods**

163 *3.1. Satellite imagery*

164 Satellite images, derived from Landsat 7/8 (2000 to 2015), and Sentinel 2 (Jan to Dec 2016), were
165 selected based on acquisition date and cloud cover such that the most meaningful scenes were identified
166 for the period of time considered in this study (Table 1). Scenes with minimum cloud cover were chosen
167 for optimum assessment of the shoreline position and also as ground control points (GCP). The spatial
168 resolution of Landsat 7/8 scenes is 20 m, while Sentinel 2 scenes offer 10 m resolution. While Landsat

169 and Sentinel imagery are provided as georeferenced products, to independently evaluate the positional
170 accuracy of each scene for shoreline change analysis, a total of five carefully considered GCPs proximal
171 to the shoreline across the study area and visible in each scene were identified and compared to the most
172 recent imagery (the control scene). This allowed to determine the relative positional error in the satellite
173 images used in this study, with RMSE ranging from 6.0 to 33.6 m, with a mean RMSE for all images
174 of 15.99 m. (Table 1).

175 Table 1: Date, RMSE, source and resolution of scenes used in this study.

Scene date	RMSE	Source	Resolution
20160104	7.7	Sentinal 2	10 m
20160314	11.14	Sentinal 2	10 m
20160403	7.82	Sentinal 2	10 m
20160503	12.78	Sentinal 2	10 m
20160622	7.65	Sentinal 2	10 m
20160801	6.67	Sentinal 2	10 m
20160811	6.01	Sentinal 2	10 m
20161030	9.44	Sentinal 2	10 m
20151218	33.64	Landsat 7/8	20 m
20151116	19.92	Landsat 7/8	20 m
20150727	17.21	Landsat 7/8	20 m
20150524	20.95	Landsat 7/8	20 m
20150217	17.45	Landsat 7/8	20 m
20100424	14.01	Landsat 7/8	20 m
20100118	21.14	Landsat 7/8	20 m
20101017	21.59	Landsat 7/8	20 m
20100203	26.78	Landsat 7/8	20 m
20051222	19.69	Landsat 7/8	20 m
20050731	20.06	Landsat 7/8	20 m
20050816	12.82	Landsat 7/8	20 m
20050715	19.26	Landsat 7/8	20 m
20050309	19.43	Landsat 7/8	20 m
20001122	14.47	Landsat 7/8	20 m
20000717	16.17	Landsat 7/8	20 m
Mean RSME	15.99		

176

177 *3.2. Shoreline change analysis*

178 Shorelines were manually digitized in ESRI ArcMap using the wet/dry line as the proxy for shoreline
179 position. The wet/dry line is accepted as an indicator of the high-water line position (Boak and Turner,
180 2005); and this is the most conspicuous and reliable shoreline proxy that can be obtained from the
181 medium-resolution satellite imagery used in this study. Discontinuities in the shoreline (i.e. river
182 mouths) were not considered in the analysis. Some scenes suffer from data gaps as a result of technical
183 problems with the scan line corrector in the Landsat 7 multispectral sensor (Fig. 2). When encountered,
184 these data gaps were filled using a subsequent scene because the gap location is different for each scene
185 (Storey et al., 2005).

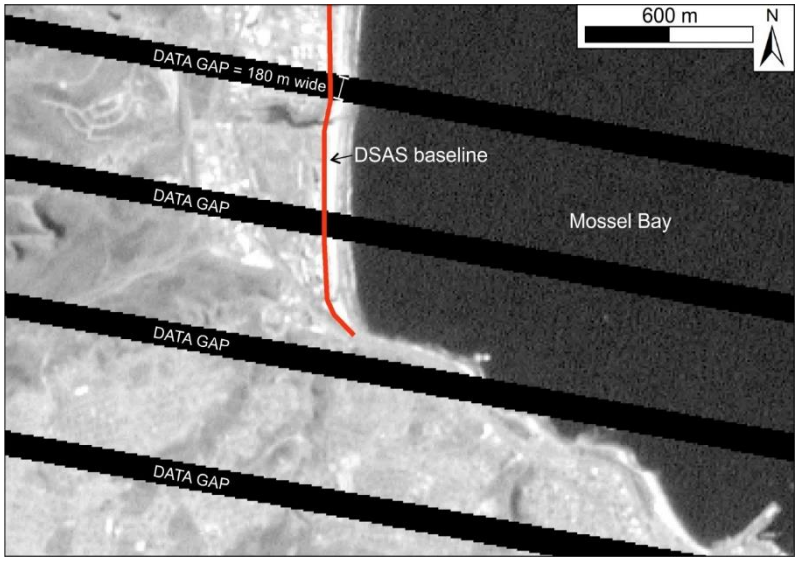

186 Fig. 2. Example of data gaps due to the Scan Line Corrector malfunction in the Landsat 7 imagery.

187

188 The Digital Shoreline Analysis System (DSAS) version 4.3 developed by the United States Geological
189 Survey (USGS) was used for the analysis of shoreline changes over time (Thieler, et al., 2009). The
190 DSAS is embedded in ESRI ArcMap and allows analysis of shoreline change using the End Point Rate
191 (EPR) method, as well as by calculating Shoreline Change Envelope (SCE), Net Shoreline Movement
192 (NSM), Weighted Linear Regression (WLR), and the uncertainty associated with the EPR (cf. Thieler,
193 et al., 2009) (Table 2).

194

195

196 Table 2: Shoreline change statistics generated by the DSAS

	Statistic	Comment
EPR	End Point Rate	Quotient of shoreline movement over time elapsed between the oldest and the youngest shoreline
SCE	Shoreline Change Envelope	A measure of horizontal distance between the proximal and distal shorelines, relative to the baseline, irrespective of age
NSM	Net Shoreline Movement	time sensitive; NSM determines the horizontal distance between the oldest and youngest shoreline
WLR	Weighted Linear Regression Rate	More reliable data are given greater emphasis when determining a best-fit line

197

198 Changes in shoreline position are related to a *baseline*, which corresponds to a reference line inshore of
199 the landward-most shoreline. Perpendicular transects spaced every 50 m and extending 200 m seaward
200 of the baseline where generated by DSAS, intersecting all the digitised shorelines; each representing a
201 time-specific shoreline position (Fig. 3). Shoreline change statistics computed by DSAS use the
202 information retrieved from the intersections in relation to the baseline position. In DSAS 4.3 the
203 computations are performed trough MATLAB executables bundled with DSAS.
204 In this study, the analysis was performed to investigate two temporal shoreline change scenarios: the
205 first scenario is a multiannual, lower temporal resolution analysis of shoreline position change from
206 2000 to 2015; while the second scenario focused on a shorter-term, higher temporal resolution analysis
207 of seasonal shoreline change in 2016.

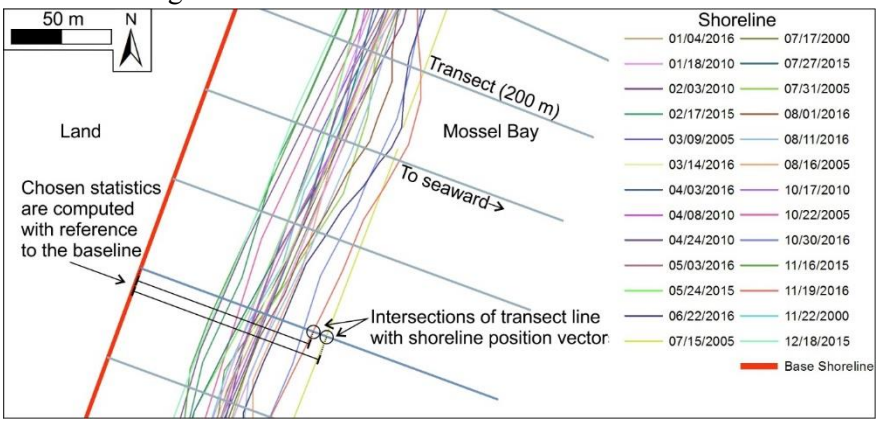

208 Fig. 3. Example of DSAS analysis. Shoreline position over time is compared to the base shoreline.

209 *3.3. Bathymetric data*

210 Regional bathymetry data were digitized in ESRI ArcMap, using soundings and isobaths of South
211 African Navy Chart 123 and gridded to a 50 m spatial resolution. High-resolution multibeam

bathymetry data within the embayment were collected from April – May 2011 using the survey vessel S/V 'GeoManzi'. During this survey, the continental shelf was mapped between depths of 10 m and 55 m below Mean Sea Level (MSL) using a 400 kHz Reson Seabat 7125 multibeam echosounder. Vessel motion was corrected using an Applanix POS MV 320 motion reference unit and positions were constrained within sub-decimeter resolution by a C-Nav Differential GPS. The survey navigation was done using QPS Qinsy software. Sound velocity profiles were collected daily within the survey area to correct the multibeam echosounder data for changes in the velocity of sound through the water column. As soundings inshore of 10 m were not available along the entire study area a depth of 15 m was chosen as the inshore data limit to ensure the model used recent high-resolution data. These survey data were gridded at a final resolution of 10 x 10 m for integration with the regional bathymetry for use in the wave modelling analysis.

3.4. Wave modelling

Wave data from two locations proximal to Mossel Bay coastline were made available by the South African WaveNet service operated by the CSIR, specifically the FA Gas Platform and Mossel Bay buoy (Fig 1). Deepwater wave conditions were obtained from the FA Gas Platform, located ca. 72 km offshore Mossel Bay in water depth of 113 m, while inshore waves, used for modelling validation, were obtained from a Waverider buoy located in the eastern section of the embayment in water depth of 24 m (Fig. 1). Wave direction was retrieved from the GOW2.0 global wave reanalysis (Perez et al., 2017). To determine nearshore wave parameters along the entire embayment, the spectral wave model SWAN (Simulating WAves Nearshore; Booij et al., 1999) was implemented using a nested modelling scheme. In the coarser regional grid (50 m resolution) SWAN was forced using the mean and 90^{th} percentile wave height and period determined from the FA Gas Platform and wave direction from the GOW2.0 dataset. The model runs for the regional grid allowed to determine the boundary conditions for the finer inshore grid (10 m resolution), which was used to characterize the nearshore wave field along the 15 m isobath. Following Matias et al., (2019) and Anfuso et al. (2020), SWAN was run in 2D stationary mode, i.e. time is removed from the simulations and the waves are propagated instantaneously across the modelling domain, using a JONSWAP spectral shape to represent the wave field and including default parameterizations for bottom friction dissipation, non-linear wave interactions, diffraction and

depth-induced breaking. The model runs were forced in the offshore boundary with the parametric wave information for mean wave conditions (wave height of 2.7 m, mean wave period of 6.6 s, wave direction 201˚) and storm wave conditions corresponding to the 90th percentile of the wave distribution (wave height of 4 m, mean wave period of 7.8 s, wave direction 218˚)

3.5 Grain size analysis

Sediment samples were collected from the active beach at 21 sites in Mossel Bay, approximately 1 km apart along the embayment, during winter (24th – 27th June, 2015). Samples were analysed using a Malvern Instrument Mastersizer 2000 particle size analyser. Replicate sample results were output from the Mastersizer 2000 to Microsoft Excel and averaged for interpretation.

4. Results

4.1. Long-term shoreline change

Changes in shoreline position in Mossel Bay over the 15-year period from 2000 to 2015 are characterized by an overall erosion pattern reflected in negative shoreline change rates, as indicated by the EPR and WLR statistics, and a generally negative NSM (Fig. 4). However, there is considerable alongshore variability in shoreline change, which is evident in all shoreline change metrics presented. In terms of the envelope of change, significantly higher shoreline variability is observed in the eastern part of the embayment (transects 350 to 570 in Fig.4), with shorelines ranging in position in excess of 80 m over the fifteen-year period (2000 – 2015). Lower shoreline variability was measured along the central and western sections of the Mossel Bay embayment (approximately in the range of 20 to 30 m for SCE), with more dynamic locations associated with the three prominent river mouths. However, when considering the results from the other variables (EPR, NSM and WLR) it becomes evident that there is relatively moderate shoreline erosion along the entire embayment over the 2000 – 2015 period, with more significant shoreline retreat in the eastern section and at a few localised hotspots (Fig. 4). This can be observed through the End Point Rate, expressed as metres per year (m/yr), which varies from - 2.5 to -3.5 m/yr in the vicinity of the Hartenbos River mouth (transects X to Y) to more than 4 m/yr at the Klein- and Groot Brak River mouths as well as at Glentana in the eastern part of the areas of the study area. Based on the NSM results, there is consistent higher variability eastward from transect

310 to the eastern end of the embayment. Although the net shoreline change displays a generally negative trend, a few accretional hotspots are also evident. The central region of the embayment, from transect 224 to 320, exhibits reduced variability despite a small net negative trend. Over the entire period of analysis, when accounting for the uncertainty in the data, the overall shoreline behaviour in Mossel Bay based on the WLR results is characterized by an average retreat of 0.8 m/yr, with a maximum shoreline retreat of 5 m/yr. Shoreline retreat is more pronounced in the western and eastern sections, with the shoreline in the centre of the embayment (transect 200 to 320) displaying very low annual rates of change.

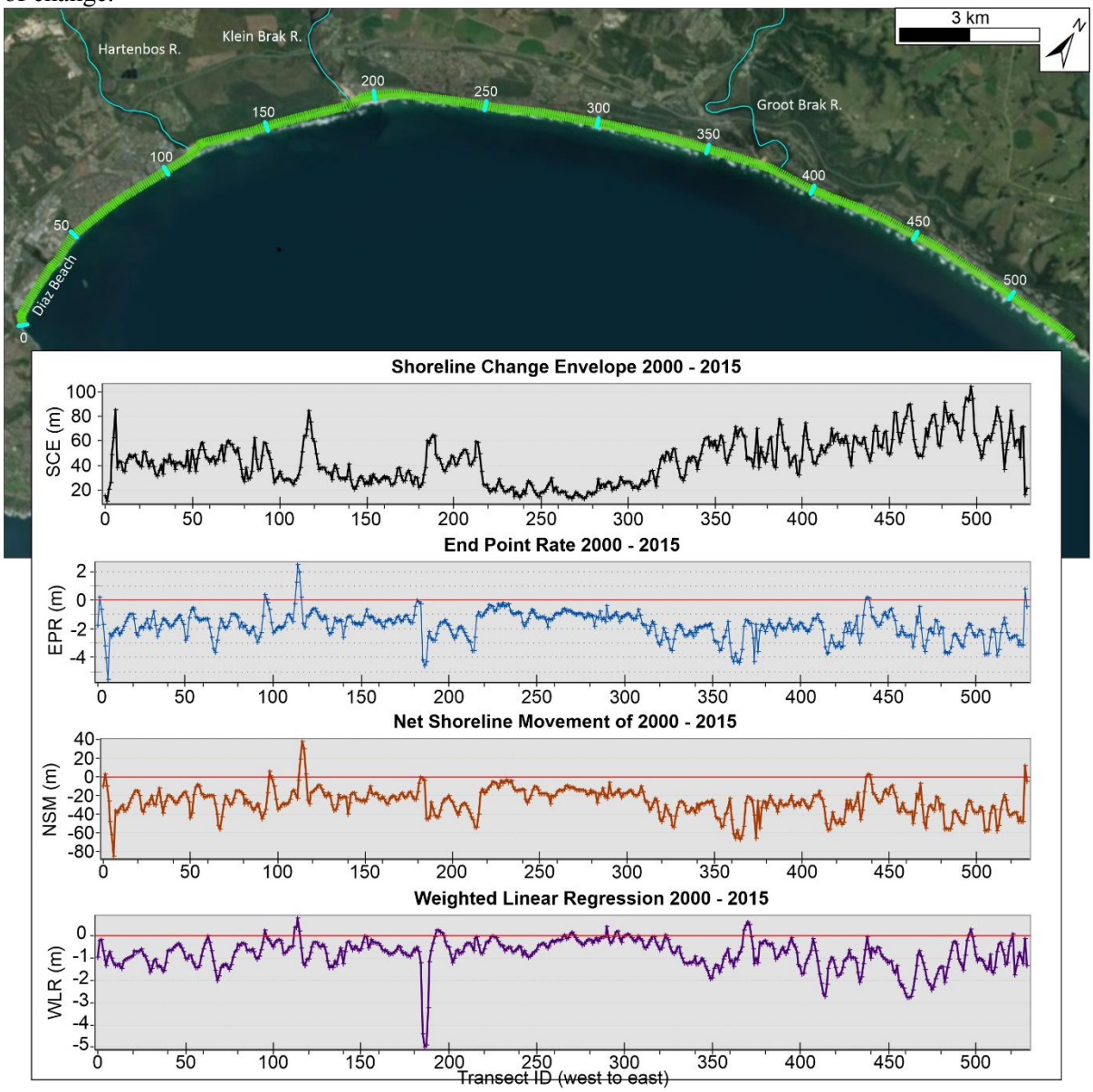

Fig. 4. Long-term shoreline change statistics in Mossel Bay, representing the period from 2000 to 2015.

278 *4.2. Short-term analysis*

279 The short-term shoreline variability along Mossel Bay, as demonstrated by the envelope of change or
280 SCE for the period between January and December 2016 (Fig. 5), is higher in the eastern section of the
281 embayment (transects 360 to 550) with values in excess of 20 m of shoreline change in this 12-month
282 period. Shoreline change is substantially less pronounced in the western to middle parts of Mossel Bay,
283 with no apparent increase in shoreline variability linked to the location of the three river mouths.
284 According to the results for the EPR, NSM and WLR, an alternating or rhythmic pattern of erosion and
285 accretion is evident in the eastern section of the embayment (eastward of transect 320). Overall, short-
286 term accretion is observed along the central and western sections of Mossel Bay, with a localised hotspot
287 of erosion in proximity to the Groot Brak river mouth. An 8 km stretch of coast that extends from Diaz
288 Beach in the southwest (transect 1 to 20) to the Hartenbos and Klein Brak Rivers towards the northeast
289 (transect 170) is dominated by overall accretion. Because shoreline change rates are computed for yearly
290 periods, the EPR and WLR mirror closely the NSM; overall there is a largely positive (seaward)
291 migration of the shoreline over the short-term. The WLR average along the embayment is 16.3 m/yr,
292 ranging from maximum erosion of -42.29 m/yr and maximum accretion of 82.05 m/yr.
293

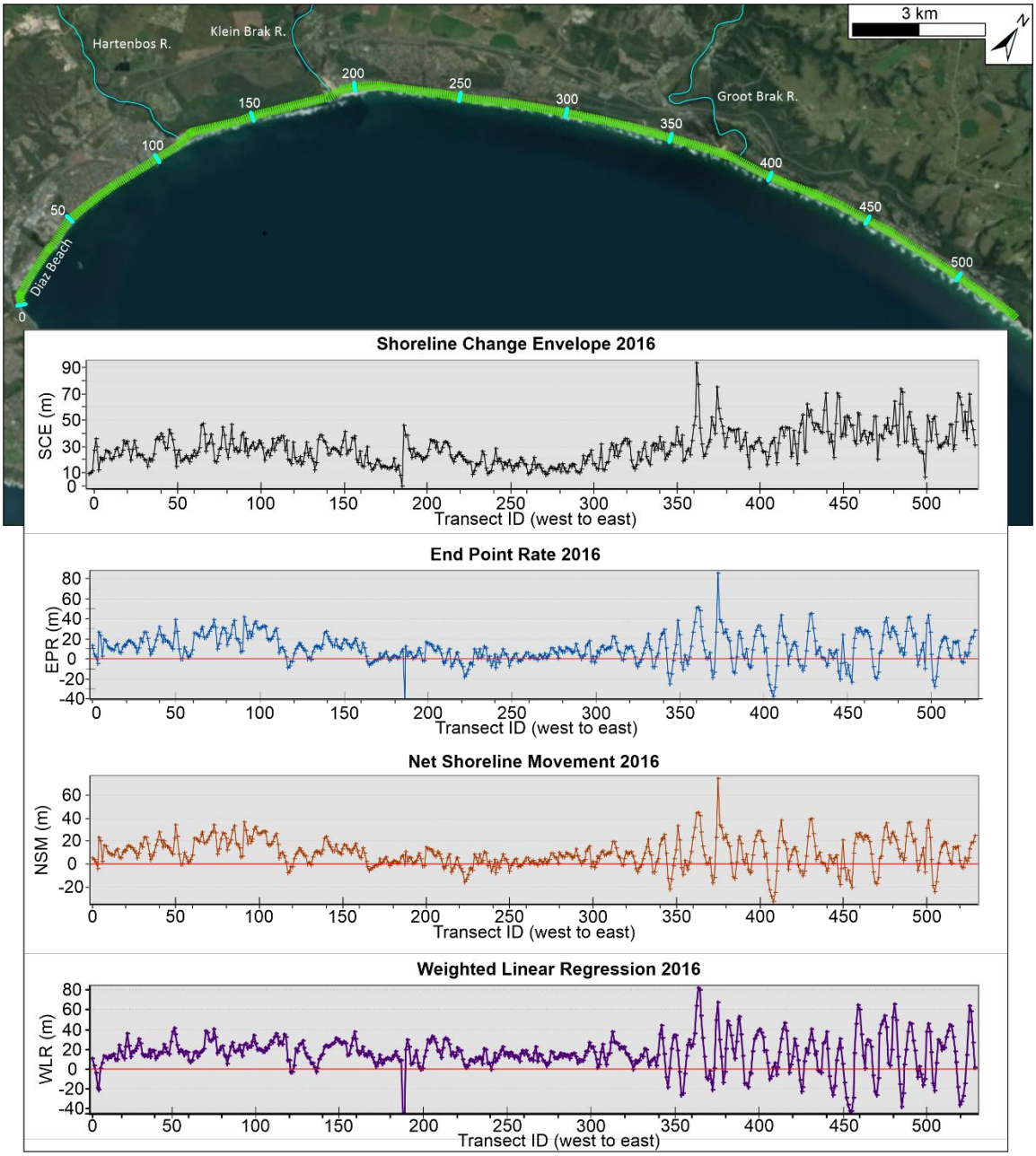

294 Fig. 5. Short-term shoreline change statistics in Mossel bay, representing the period from January to
295 December 2016.

296 *4.3. Nearshore wave conditions*

297 Alongshore variability in nearshore wave conditions determined from wave modelling shows very
298 similar trends for mean and storm wave conditions, characterized by a gradual increase in wave height
299 towards the eastern section of the embayment (Fig. 6). Modelled mean and storm wave parameters are
300 in close agreement with the data for equivalent conditions obtained from the nearshore wave buoy
301 located in the protected western section of the bay. During both mean and storm conditions, the
302 prominent headland of Cape St. Blaize (Fig. 1) affords a significant degree of protection to the western

303 sector of the embayment, given that both mean and storm waves approach this coastline from a SSW to
304 SW direction. The shadow effect of this headland leads to a significant gradient in wave height along
305 the embayment, with wave heights in the protected western sector approximately 50% lower than in the
306 exposed western sector for both wave conditions. Nearshore wave heights along the 15 m isobath
307 contour reach approximately 2 (3) m for mean (storm) conditions in the more energetic western sector,
308 gradually decreasing along the central section of the embayment, where they reach between 2.5 and 2
309 meters during storms (Fig. 6).
310

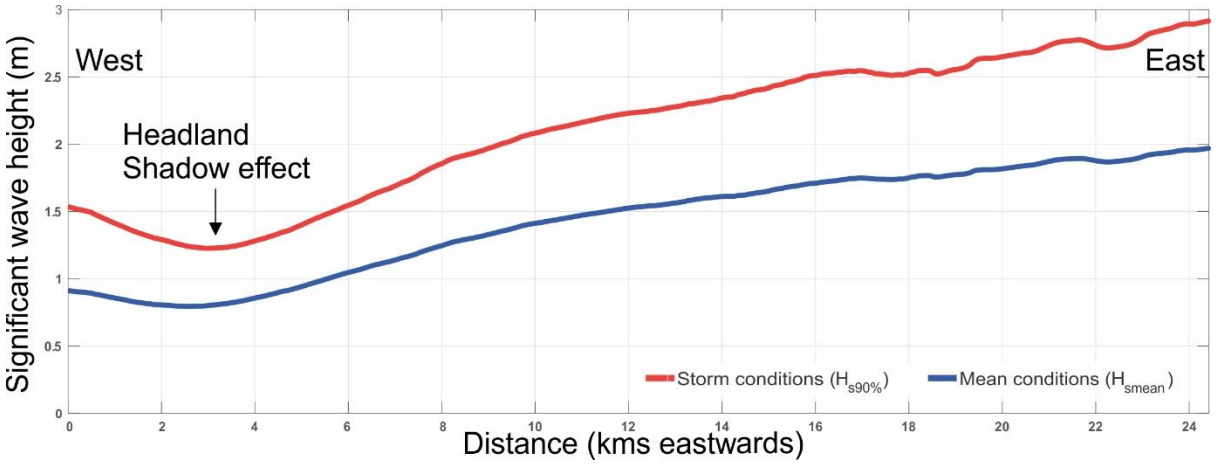

311 Fig. 6. Alongshore gradient in mean and storm nearshore wave heights for Mossel Bay.

312 *4.4. Grain size*

313 Sediment analysis in 21 locations along the embayment reveals a dominance of medium sand (250 –
314 500 um) in all but four sites (Fig 7). These four beaches (P10, P12, P13 and P14) are located in the
315 central part of the embayment; three are dominated by coarse sand (500 – 1000 µm) while the fourth
316 (P14) exhibits a higher percentage of very coarse sand (1000 – 2000 µm). Regarding the finer sediment
317 fractions, fine sand (125 – 250 µm) is more prevalent in the western sector of the embayment, with a
318 sharp reduction towards the the central and eastern sectors. Significant but not dominant contributions
319 from very coarse sand (>10%) is noted at five sites; three in the coarse central region and one example
320 in the west and east respectively. Sorting increases substantially from the central to the eastern sector
321 of the embayment, with sediment distribution in most sites between P15 and P21 represented in over
322 60% by medium sand (250 to 500 µm).

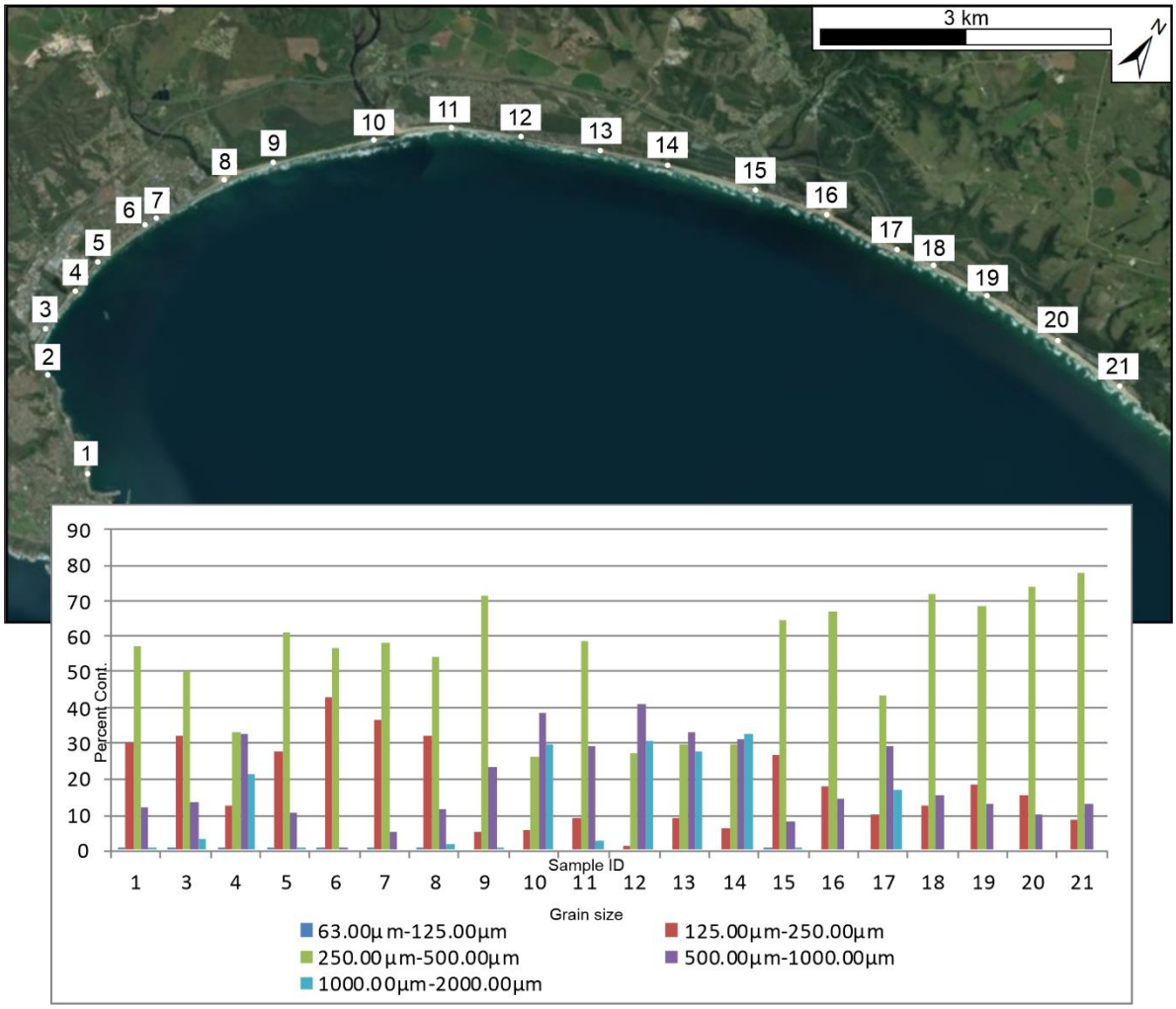

Fig 7. Distribution of grain size classes along Mossel Bay. P2 is a rock outcrop with no beach (devoid of sediment).

4.5. Beach and nearshore rock outcrops

Three well-defined areas of inter to subtidal rocky outcrop are evident along the beach and nearshore areas of Mossel Bay (Fig. 8). The western outcrop (Platform A) is the smallest, roughly half the size of the central platform (Platform B), with the eastern platform (Platform C) covering for a much wider area (Table 3). Platform A extends for approximately 430 m offshore from the shoreline, with a seaward edge characterised by a steep gradient (ca. 1.5°) between ~9.5 m and ~13 m depth. Seaward of the platform edge, the gradient is reduced to 0.3°. Platform B shares most of the same geometrical characteristics of Platform A, apart from a much steeper platform edge (ca. 3.8°). Platform C, in the east, is marginally wider that Platforms A and B, and presents substantial alongshore variability, with a

335 steeper platform gradient in the central section. Seaward of the platform edge, the slope of the nearshore
336 is steeper in this section of the embayment.
337 The surface of Platform C hosts an elongated coast parallel sandbar covering ca. 0.5 km^2 and extending
338 5 km across the outcrop (Fig. 8). In the west the bar merges with the nearshore sediment wedge as the
339 outcrop relief diminishes, while to the east the sandbar attaches to the beach; the underling rock crops
340 out 300 m offshore. Platform A is generally restricted to the subtidal area of the nearshore, while
341 Platforms B and C extend to the upper intertidal zone. All three outcrop platforms extend seaward across
342 the upper shoreface. Platform A is associated with distinct sand patches which overlie the consolidated
343 rock surface. Platform B is draped by unconsolidated sands in the east, however, sediment cover thins
344 rapidly in the middle and eastern sections of the outcrop that terminates around the Klein Brak River
345 mouth. Outcrop of Platform C decreases in relief above the adjacent sediment wedge from ca. 8 m in
346 the east, to 4 m off the central platform and finally merging with unconsolidated sands at the western
347 extent.
348 **Table 3:** Rocky platform geometry and geomorphological context

ID	Area	Platform edge elevation difference	Platform edge gradient	Shoreline to platform edge	Seaward gradient	Outcrop location
A	0.8 km^2	3.5 m	1.5°	430 m	0.3°	Nearshore/Sub-tidal
B	1.5 km^2	4.5 m	3.8°	430 m	0.3°	Nearshore/Intertidal
C	3.6 km^2	8 m(Eastern) 8 m (Central)	1.9° (Eastern) 2.6° (Central)	500 m (Eastern) 530 m (Central)	0.6°	Nearshore/Intertidal

349

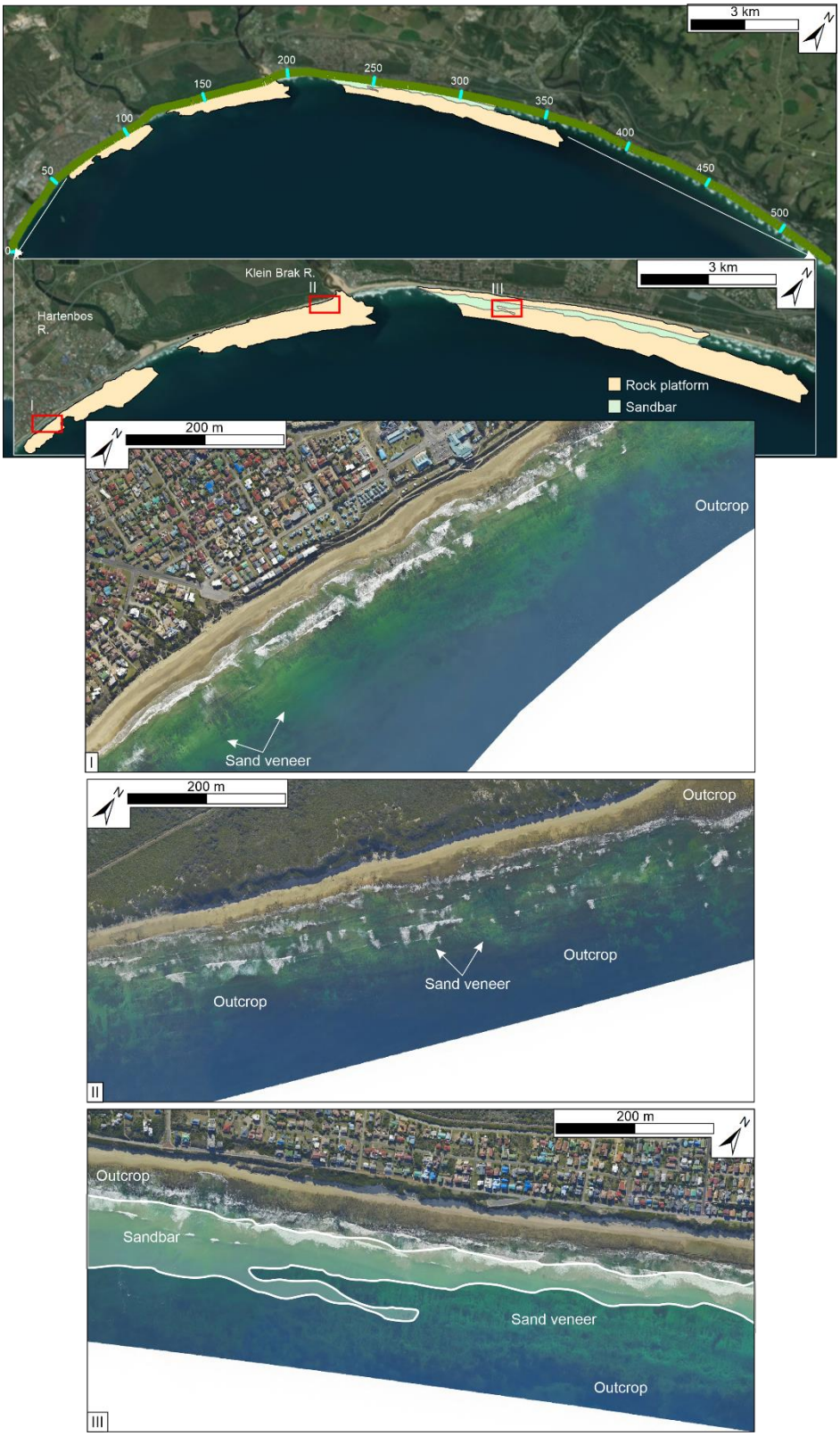

350 Fig. 8. Prominent beach and nearshore rocky platforms along Mossel Bay. The platforms are typically
351 covered by a thin sand veneer, which becomes a distinctive sandbar in the easternmost platform.

352

353

5. Discussion

5.1 *Wave forcing and shoreline change*

The wave conditions in Mossel Bay are forced by south-westerly swells from the Southern Ocean for both mean and storm waves. Under both conditions a defined wave shadow zone develops in response to diffraction and refraction of waves around Cape St. Blaize, leading to a marked alongshore gradient in wave heights along the embayment (Fig. 6). When comparing the long-term shoreline change patterns with wave forcing along Mossel Bay, there isn't a clear association between rates of change for the EPR and NSM metrics and higher wave heights in the more exposed eastern sector. However, this exposed sector does exhibit a consistently higher envelope of change (SCE), indicating that in this sector of Mossel Bay, shoreline variability over the 15 period between 2000 and 2015 is higher, although such increased variability is not reflected in increased shoreline erosion (Fig. 4). When considering short-term shoreline change throughout the year of 2016, the association between higher wave forcing and increased shoreline variability becomes much more pronounced (Fig. 5), with a clear transition from relatively moderate SCE, EPR and NSM in the western and central sectors of the embayment, in contrast with a much wider envelope of change and large variability in shoreline change rates in the eastern sector (transects 330 to 550). These results are not unexpected, and association between shoreline change and hydrodynamic forcing at regional scales is well established (e.g Castelle et al., 2018; Carvalho et al., 2020). However, by exploring in more detail the alongshore changes in wave forcing as a driver of shoreline variability in medium scale coastal embayments, this work highlights the role of spatial variability in hydrodynamic forcing, which can both contrast and complement temporal variability in wave forcing in driving long to short-term shoreline change (Carvalho et al., 2020).

5.2 Geological framework and shoreline change

In addition to spatial and temporal variability in hydrodynamic forcing, spatial variability in coastal geomorphology can also exert a significant influence or indeed control to a large extent the evolution of sedimentary coasts (Cooper et al, 2018). Often termed geological control, the presence of outcropping or subcropping rocky surfaces within sandy shorelines and their influence in beach dynamics has been increasingly recognized (Gallop et al., 2020).

382 Along Mossel Bay there are extensive intertidal to subtidal rock out/subcrops in the form of beachrock
383 and/or aeolianite, which are comparable to rock-platform or reef perched beaches (Gallop et al., 2011).
384 The location of these platforms relative to mean sea level and within the embayment plays an important
385 role in shoreline change across spatial and temporal scales. The western platform (Platform A) occupies
386 the nearshore to sub-tidal level, seldom exposed on the active beach (intertidal). Platforms B and C,
387 central and eastern respectively, both extend further inshore to occupy the active beach and intertidal
388 zone. Much of Platform C is exposed during low tides as a wave-cut platform. In all three cases it is
389 very likely that the rock platforms extend landward and underlie the unconsolidated active beach. The
390 influence of the rock platforms in the spatial patterns of shoreline change is consistent across temporal
391 scales, although more pronounced for platforms B and C. This is evidenced by reduced long-term
392 variability in shoreline position (based on SCE) and minimal rates of change (according to EPR, WLR),
393 for the section between profiles 130 to 180 for Platform B and transects 220 to 320 for Platform C (Fig.
394 4). In terms of short-term shoreline variability, the reduction of shoreline variability due to the presence
395 of the rock platform is more noticeable in the reduced rates of shoreline change in the sector fronting
396 platform B and C (transects 170 to 320 – Fig. 5).
397 While the precise morphodynamic mechanisms by which the rock platforms influence shoreline change
398 are beyond the scope of this study, based on previous investigations into the influence of nearshore
399 reefs on hydrodynamics and sediment transport in sandy beaches (e.g. Cleary et al., 1996; Larson and
400 Kraus, 2000; Vousdoukas et al., 2007; Storlazzi et al., 2010; Velegrakis et al., 2016), it is reasonable to
401 suggest that the three platforms enhance wave attenuation, reducing the energy of waves that reach the
402 coastline contribution to a more stable or shoreline position. Under storm conditions the protective role
403 of shore platforms may be less significant, as nearshore rocky outcrops also contribute to enhance the
404 infragravity wave energy component that reaches the beach (Gallop et al., 2020). A direct association
405 between the rock platforms and shoreline change is further complicated by the fact that platforms in
406 Mossel Bay vary in size, morphology and position within the embayment, but also because their
407 seaward edge is heterogenous and offshore of the platforms a reef complex is found at depths between
408 20 and 45 m (Cawthra et al., 2018), which interferes and modifies the propagation of nearshore waves,
409 particularly during storm conditions.

410 The embayment of Mossel Bay is considered sediment starved compared to the adjacent regions owing
411 to a combination of low siliciclastic supply and transport regimes within the regional geological control
412 (headland and embayment framework) (Birch, 1980). Active beach sediments are dominated by quartz
413 and carbonate clasts reflecting the geology of the hinterland catchments and Holocene sediment wedge,
414 and biological productivity of the adjacent Ocean, rich in carbonate-producing organisms, respectively.
415 Active beach sedimentological characteristics complement those of the modern shoreface which are
416 described by coarse grained bioclastic sediment, fine to medium-sand dominated shelf sands, silty mud
417 and mud (Cawthra, 2014), although lacking the finer fraction. There are notable sedimentological
418 variations across the embayment manifest as three zones; western, central and eastern. In the west
419 (sample localities 1 –9), encompassing Platform A, medium and fine sand offer the greatest contribution
420 to active beach grainsizes with less contribution, if any, from coarse and very coarse clasts (Fig. 7).
421 Some regions (i.e., between sites 1 and 2) are, however, largely devoid of sediment with bioclastic
422 debris (shell hash to entire shells) covering the intertidal and supratidal outcrop. The central sector (10
423 –14), including Platforms B and C, is associated with greater contributions of coarse sediment compared
424 to the western zone. The eastern zone (15 –21), devoid of intertidal outcrop, is dominated by medium
425 sand with little coarse material and only one site (17) recording very coarse clasts. Platform C position
426 relative to the beach changes spatially (Fig. 8), with no significant outcrop extending towards the active
427 beach from 17 through 21, which suggests that coarser sediment is not being actively sourced from the
428 platform to the beach as in the eastern and central sectors. The change in grainsize composition along
429 Mossel Bay is therefore interpreted as driven by both rock platform characteristics and hydrodynamic
430 forcing, with variable contribution of the platforms as source of coarse beach sediment and transport
431 pathways that reflect the influence of platform position in relation to the beach. Samples were collected
432 during calm sea conditions thus represent such conditions. Localised pebble and shell lags are common,
433 though not resolved at 1 km sample spacing hence they are not included in this regional account. As the
434 adjacent contemporary shoreface comprises coarse grained bioclastic sediment, fine to medium-sand,
435 it is unlikely that the beach composition would change significantly during storm events. There may,
436 however, be local winnowing of the finer fraction creating temporarily course beaches and pebble lags.
437 Post-storm periods would allow re-introduction of the finer fraction to the system once more.

438 *5.3 Integrated model of shoreline change*

439 Long-term shoreline change metrics indicate that the embayment of Mossel Bay is undergoing net
440 erosion, with WRL providing a more reliable indication compared to EPR, as the latter does not consider
441 uncertainty (Thieler et al., 2009). While the mean relative positional error is 15.99 m, for most images
442 it is smaller than the image resolution (20 m for Landsat and 10 m for Sentinel - Table 1). This suggests
443 subpixel geometric mismatch between images, which is often identified in multiscale satellite data
444 analysis (Wu et al., 2021). Error of this magnitude naturally reduce the accuracy of the shoreline change
445 analysis, however, when considered in the context of large shoreline change envelopes and, particularly,
446 the incorporation of uncertainty in the determination of shoreline change rates using weighted linear
447 regression, their impact on the accuracy of the shoreline change analysis becomes less significant. Based
448 on these metrics, shoreline erosion observed in Mossel Bay is relatively minor, averaging -0.8 m per
449 year (based on the 2000 – 2015 WLR), compared to the average retreat of the African East coast which
450 approximates -1.4 m per year (Mentaschi et al., 2018), but closer to the values computed automatically
451 for Mossel Bay during the period from 1986 to 2016 by Luijendijk et al. (2018). Over the short-term
452 timescale and considering a single year (2016), our results indicate that average accretion of 16.3 m
453 based on the WLR. In both long and short-term analysis there is district compartmentalisation of
454 shoreline responses described by three sub-cells; Western, Central and Eastern (Fig. 9). Transect ca.
455 325 to 533 describes an eastern section within the embayment (ca. 9.7 km). This eastern sub-cell
456 manifests significant variation in the envelope and rates of change. Thus, shoreline position is very
457 dynamic on an annual to seasonal scale. The western extent of this dynamic sub-cell coincides with the
458 eastern limit of the intertidal to subtidal rock platform. The of absence of this intertidal rock platform
459 continues to the limit of the embayment at the eastern sea cliffs. Westward of transect 125, through to
460 transect 1, we identify a western sub-cell. This sub-cell evidences shoreline change rates that are lower
461 than the eastern sub-cell, but higher than the central sub-cell that lies in between. Medium sand
462 dominates the beach in the eastern and western sub-cells, while the central sub-cell is characterized by
463 coarser and poorly sorted sediment.

464 The eastern sub-cell is associated with high variability in shoreline position over the long and short-
465 term with changes of up to 100 m between shoreline position. This cell experiences the greatest
466 significant wave heights across normal and storm conditions, and a normal wave approach. The
467 irregular to rhythmic variation in shoreline position, particularly in the short-term analysis, suggests
468 that shoreline change in this sector may be associated to the development and migration of megacusps,
469 creating alternating hotspots or erosion and accretion (Thornton et al., 2007).

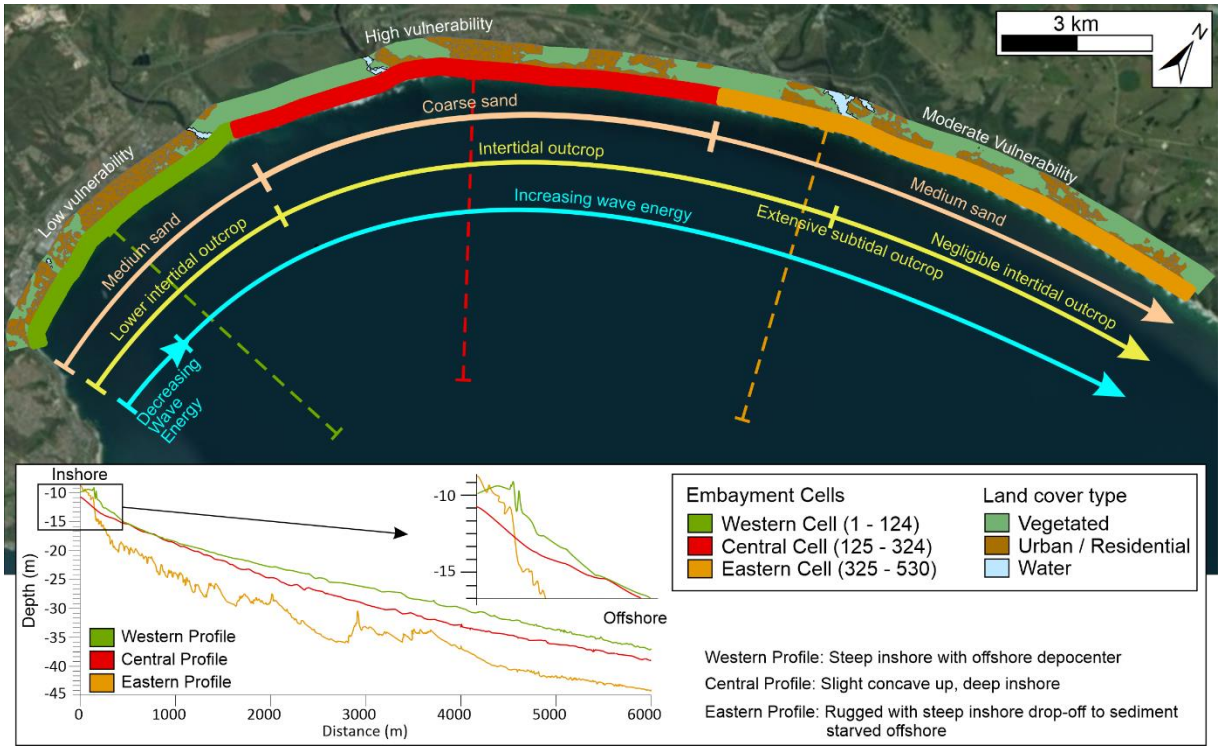

470 Fig 9: Conceptual model of shoreline change in Mossel Bay based on three distinct sub-cells. Coast-
471 perpendicular profiles highlight variations in shoreface and offshore geometry.

472 The three sub-cells demonstrate varied coastal response to hydrodynamic forcing along the embayment,
473 however, wave forcing is not the single control. Despite the increase of wave energy from the western
474 to eastern across the embayment, the shoreline response is not linear. Rather, the presence or absence
475 of rock outcrops plays a key role in modulating shoreline change. In particular, intertidal rock platforms
476 are integral to shoreline dynamics over time, influencing the dynamics and the sediment that is found
477 along the embayment. Coast-perpendicular bathymetry profiles show variation in geometry that may
478 result from interactions between cells (Fig. 9). The eastern profile is rugged, relatively sediment starved
479 and subject to increased wave exposure, hence dominated by outcrop (cf. Cawthra et al., 2015) and
480 deeper offshore than the central and western areas The eastern shoreface is narrower and steeper (Fig.

9), shoaling rapidly towards the shoreline. Resembling the equilibrium surface of Anthony and Aagaard (2020), the central profile is concave upward, steepening across the upper shoreface. The upper shoreface of the western profile shoals more rapidly than that of the central cell, and appears to accumulate sediment across the lower shoreface to offshore acting as a depocentre within the western embayment. This western cell is subject to lower wave energy and presents lower vulnerability than the cells to the east. This likely accounts for the preferential accumulation of sediment in this region, although the mechanisms remain unknown. It is plausible that either sediment is winnowed from the central and eastern cells bypassing the eastern headland and leaving the western cell shoaler. Alternatively, sediment eroded and transported from the eastern and central regions is deposited within the sheltered western embayment, under specific conditions at least, thus increasing sediment thickness relative to the central and eastern cells.

If we consider the potential impacts of shoreline change along Mossel Bay in relation to the development of the coastal zone, as determined by the residential areas and urban infrastructure, while the western sub-cell is highly developed it experiences minor shoreline change and is exposed to less energetic forcing, making it the least vulnerable sub-cell to potential damages associated with shoreline change. The eastern sub-cell exhibits marked shoreline variability and significant coastal development, but buildings and infrastructure are located landward to the frontal dune system, making this a zone of moderate vulnerability. Compared to the eastern and western sub-cells, the beach in the central sub-cell is narrower and the frontal dune steeper, with significant coastal infrastructure (e.g. roads and parking) and buildings located on top of the frontal dune (Fig. 8). This implies that even relatively small changes in shoreline position can have potentially severe impacts, suggesting that this region may present higher coastal vulnerability than the remaining sectors of Mossel Bay. Thus, development within this zone is not recommended owing to the likelihood of infrastructural damage.

While entirely rocky coasts are typically more stable and resistant to change at annual to decadal timescales, coastal areas comprising a mix of rocky and sedimentary coastal landforms are substantially more complex, with implications for shoreline change and coastal vulnerability. In the last decade infrastructure placed along sections of the central sub-cell has been damaged extensively as a result of seasonal shoreline migration. These changes in shoreline position, although the lowest within the entire

509 embayment, interact more closely with existing infrastructure increasing dune instability and erosion,
510 enhancing coastal risk. This association has implications for characterizing coastal hazards and
511 delineating high risk zones other coastal areas, as shoreline change patterns alone provide an incomplete
512 view of coastal dynamics. Thus, regional coastal setback lines developed without a holistic approach
513 may not adequately account for hazards associated with local scale variation in embayment
514 characteristics. Hence, enhanced local knowledge generation must outpace the development of this
515 dynamic zone to enable sound coastal zone management (Stive et al., 2002). Ideally, long-term trends
516 are best described by analysis of long-term shoreline position records. Such records would encapsulate
517 dramatic short-term, as well as persistent long-term changes along unconsolidated shorelines enabling
518 analysis at the highest possible spatio-temporal resolution (Castelle et al., 2021).There is much debate
519 over the fate of sandy shorelines (cf. Vousdoukas et al., 2020 and Cooper et al., 2020), this contribution
520 highlights the need for local-scale studies to meaningfully describe local changes, risks and hazards in
521 response to local conditions (cf. Guisado-Pintado and Jackson, 2019). While global or continental-scale
522 contributions provide a low-resolution high-level overview of coastal issues (Vousdoukas et al., 2022),
523 local-scale, high resolution studies are paramount to informing coastal management and policy makers.

524 **6. Conclusion**

525 Digital shoreline analysis has been employed to describe shoreline trends over a period of 15 years.
526 Over the study period, the Mossel Bay embayment is relatively stable, with no significant signs of
527 extensive accretion or erosion. The long-term end point rate does, however, suggest that there is minor
528 shoreline erosion (average of -1.75 m/yr) along the embayment as a whole for the period between 2000
529 and 2015. The short-term analysis suggests that the shoreline position is susceptible to rapid migration
530 on a seasonal scale, particularly in response to episodic changes driven by megacusp migration. Erosion
531 and accretion hotspots are related to areas proximal to river mouths, megacusps, and areas where the
532 highly dynamic shoreline behaviour is constrained by rocky platforms and unable to freely adjust to
533 variation in forcing.

534 Alongshore variation in wave forcing is an important driver of coastal processes along Mossel Bay,
535 however, shoreline change is not directly related to the wave conditions along the embayment. Rather,
536 based on the integration of wave forcing, shoreline change, sediment characteristics and presence of

intertidal and subtidal rock platforms, we propose that Mossel Bay is divided into three sub-cells in terms of coastal processes and coastal vulnerability (Western: Dias Beach to the eastern bank of the Hartenbos River, Central: eastern bank of the Hartenbos River to Tergniet, Eastern: Tergniet to Glentana). The shoreline in the eastern and western cells is more variable than the central cell with regards to envelopes and rates of change. Hazards to coastal development and infrastructure are associated with the location of such infrastructure rather than the specific patterns of extensive shoreline change. Small changes in shoreline positon within an energetic embayment have resulted in loss of infrastructure, but little loss of sandy beach area in the long-term. Hence, future development along comparable energetic sandy coasts must be critically analysed from a local coastal geomorphological perspective that considers seasonal, episodic and short-term variation within the geospatial context of the site, and on management timelines.

Acknowledgments

The geophysical datasets collected for this project were funded by the National Geographic Society Expeditions Council (Grant number EC0482-10) and the Council for Geoscience Annual Technical Programme (Project number ST-2011-1139). We acknowledge the CSIR, Stellenbosch, for wave data which was collected on behalf of the Transnet National Port Authority, and PETROSA for kindly providing wave buoy data, as well as the Environmental Hydraulics Institute (IHCantabria) for the modelled wave directions data from the GOW2.0 hindcast dataset. This manuscript contains modified Copernicus Sentinel 2A data [2016] (European Space Agency), as well as Landsat imagery (U.S. Geological Survey).

565 **References**

566 Anthony, E.J., Aagaard, T., 2020. The lower shoreface: Morphodynamics and sediment connectivity
567 with the upper shoreface and beach. Earth-Sci. Rev. 210, http://dx.
568 doi.org/10.1016/j.earscirev.2020.103334.
569 Alexandrakis, G., Manasakis, C. and Kampanis, N.A., 2015. Valuating the effects of beach erosion to
570 tourism revenue. A management perspective. Ocean & Coastal Management, 111(Supplement
571 C): 1-11.
572 Anfuso G, Loureiro C, Taaouati M, Smyth T, Jackson D., 2020. Spatial Variability of Beach Impact
573 from Post-Tropical Cyclone Katia (2011) on Northern Ireland's North Coast. *Water*,
574 12(5):1380.
575 Birch, G.F., 1980. Nearshore Quaternary sedimentation off the south coast of SA (CT to PE). Geological
576 Survey Bulletin 67, 20pp
577 Boak, E.H. and Turner, I.L., 2005. Shoreline Definition and Detection: A Review. *Journal of Coastal*
578 *Research,* 21(4), 688–703. West Palm Beach (Florida), ISSN 0749-0208.
579 Booij, N.; Ris, R.C.; Holthuijsen, L.H. A third-generation wave model for coastal regions: 1. Model
580 description and validation. J. Geophys. Res. 1999, 104, 7649–7666.
581 Brew, D.S., Guthrie, G., Walkden, M. and Battalio, R.T., 2011. Sustainable coastal communities: the
582 use of crenulate bay theory at different scales of coastal management. Littoral 2010 – Adapting
583 to Global Change at the Coast: Leadership, Innovation, and Investment: 06005.
584 Burningham, H., Fernandez-Nunez, M., 2020. Shoreline change analysis. In Jackson, D.W.T. and Short,
585 A.D. (Eds), Sandy Beach Morphodynamics. Elsevier, pp. 439-460.
586 Carapuço, M.M., Taborda, R., Silveira, T.M., Psuty, N.P., Andrade, C. and Freitas, M.C., 2016. Coastal
587 geoindicators: Towards the establishment of a common framework for sandy coastal
588 environments. Earth-Science Reviews, 154(Supplement C): 183-190.
589 Carter, R.W.G., Woodroffe, C.D., 1997. Coastal Evolution: Late Quaternary Shoreline
590 Morphodynamics. Cambridge University Press.

591 Carvalho, B.C., Dalbosco, A.L.P., Guerra, J.V., 2020. Shoreline position change and the relationship to
592 annual and interannual meteo-oceanographic conditions in Southeastern Brazil. Estuarine,
593 Coastal and Shelf Science, 235, 106582
594 Castelle, B., Guillot, B., Marieu, V., Chaumillon, E., Hanquiez, V., Bujan, S., Poppeschi, C., 2018.
595 Spatial and temporal patterns of shoreline change of a 280-km high-energy disrupted sandy
596 coast from 1950 to 2014: SW France. Estuarine, Coastal and Shelf Science, 200, 212–223.
597 Castelle, B., Masselink, G., Scott, T., Stokes, C., Konstantinou, A., Marieu, V., Bujan, S., 2021.
598 Satellite-derived shoreline detection at a high-energy meso-macrotidal beach. Geomorphology
599 383, 107707. https://doi.org/10.1016/j.geomorph.2021.107707
600 Cawthra, H.C., 2014. The marine geology of Mossel Bay, South Africa. University of Cape Town.
601 http://hdl.handle.net/11427/8697
602 Cawthra, H.C., Compton, J. S., Fisher, E. C., MacHutchon, M.R., Marean, C. W., 2015. Submerged
603 terrestrial landscape features off the South African south coast. In: Harff, J., Bailey, G., Lüth
604 F. (Eds.) Geology and Archaeology: Submerged landscapes of the continental shelf. Special
605 Publication of the Geological Society of London 411, 219-233.
606 Cawthra, H.C., Anderson, R.J, de Vynck, J., Fisher, E.C., Jacobs, Z., Jerardino, A., Kyriacou, K.,
607 Marean, C.W, 2020. Migration of Pleistocene shorelines across the Palaeo-Agulhas Plain:
608 evidence from dated sub-bottom profiles and archaeological shellfish assemblages. Quaternary
609 Science Reviews 235, 106107. https://doi.org/10.1016/j.quascirev.2019.106107
610 Cleary, W.J., Riggs, S.R., Marcy, D.C., Snyder, S.W., 1996. The influence of inherited geological
611 framework upon a hardbottom-dominated shoreface on a high-energy shelf, Onslow Bay, North
612 Carolina, USA. Special Publication, 117. Geological Scociety, London pp. 249 – 266.
613 Cooper, J.A.G., 2001. Geomorphological variability among microtidal estuaries from the wave-
614 dominated South African coast. Geomorphology 40, 99-122.
615 Cooper. J.A.G., Green, A.N., Loureiro, C., 2018. Geological constraints on mesoscale coastal barrier
616 behaviour. Global and Planetary Change, 168, 15-34.

617 Cooper, J.A.G., Jackson, D.W.T., Navas, F., McKenna, J., Malvarez, G., 2004. Identifying storm
618 impacts on an embayed, high-energy coastline: examples from western Ireland. Marine
619 Geology 210, 261-280.
620 Cooper, J.A.G., Masselink, G., Coco, G., Short, A. D., Castelle, B., Rogers, K., Anthony, E., Green, A.
621 N., Kelley, J. T., Pilkey, O. H., Jackson, D. W. T., 2020. Sandy beaches can survive sea-level
622 rise. *Nat. Clim. Chang.* **10,** 993–995. https://doi.org/10.1038/s41558-020-00934-2
623 Davies, J.L., 1980. Geographical variation in coastal development. Longman, New York, 212 pages.
624 Del Rio, L., Benavente, F.J., 2013. Shoreline change patterns in sandy coasts. A case study in SW Spain.
625 Geomorphology 196, 252–266.
626 ETC CCA. Methods for Assessing Coastal Vulnerability to Climate Change Technical Paper 1/2011.
627 Available online: http://cca.eionet.europa.eu/docs/TP_1-2011 (accessed on 14 January 2019).
628 Ferreira, O., 2005. Storm Groups versus Extreme Single Storms: Predicted Erosion and Management
629 Consequences. Journal of Coastal Research, SI42, 221-227.
630 Flemming, B.W. and Martin, K.A., 2018. The Tsitsikamma coastal shelf, Agulhas Bank, South Africa:
631 example of an isolated Holocene sediment trap. Geo-Mar Lett 38: 107.
632 https://doi.org/10.1007/s00367-017-0507-5
633 Gallop, S.L., Kennedy, D.M., Loureiro, C., Naylor, L.A., Muñoz-Pérez, J.J., Jackson, D.W.T.,
634 Fellowes, T.E., 2020. Geologically controlled sandy beaches: Their geomorphology,
635 morphodynamics and classification. Science of the Total Environment, 731, 139123.
636 Guisado-Pintado, E. Jackson, D. W. T., 2019. Coastal Impact From High-Energy Events and the
637 Importance of Concurrent Forcing Parameters: The Cases of Storm Ophelia (2017) and Storm
638 Hector (2018) in NW Ireland. Frontiers in Earth Science, 7. DOI=10.3389/feart.2019.00190
639 Harley, M.D., Turner, I.L., Short, A.D., 2015. New insights into embayed beach rotation: The
640 importance of wave exposure and cross-shore processes, J. Geophys. Res. Earth Surf., 120,
641 1470–1484, doi:10.1002/2014JF003390.
642 Jackson, D.W.T., Short, A.D., 2020. Introduction to beach morphodynamics. In Jackson, D.W.T. and
643 Short, A.D. (Eds), Sandy Beach Morphodynamics. Elsevier, pp. 1-13.

644 Larson, M., Kraus, N.C., 2003. Representation of non erodible (hard) bottoms in beach profile change
645 modelling. Journal of Coastal Research 1 – 14.
646 Luijendijk, A., Hagenaars, G., Ranasinghe, R., Baart, F., Donchyts, G. and Aarninkhof, S., 2018. The
647 State of the World's Beaches. Scientific Reports, 8(1): 6641.
648 Phillips, M.R., Jones, A.L., 2006. Erosion and tourism infrastructure in the coastal zone: problems,
649 consequences and management. Tour. Manag. 27, 517-524.
650 Malan, J.A., 1990. The stratigraphy and sedimentology of the Bredasdorp Group, southern Cape
651 Province. Unpublished M.Sc. Thesis, University of Cape Town, South Africa, 197 pp.
652 Martin, A.K., Flemming, B.W., 1987. Aeolianites of the South African coastal zone and continental
653 shelf as sea-level indicators. South African Journal of Science 83, 507-508.
654 Mather, A. A., Garland, G. G. and Stretch, D. D. (2009). Southern African sea levels: corrections,
655 influences and trends. African Journal of Marine Science, 31, 145-156.
656 Matias, A.; Carrasco, A.R.; Loureiro, C.; Masselink, G.; Andriolo, U.; McCall, R.; Ferreira, O.;
657 Plomaritis, T.A.; Pacheco, A.; Guerreiro, M. (2019). Field measurements and hydrodynamic
658 modelling to evaluate the importance of factors controlling overwash. *Coast. Eng.*, *152*,
659 103523.
660 McLaughlin, S., Cooper, J.A.G., 2010. A multi-scale coastal vulnerability index: A tool for coastal
661 managers? Environmental Hazards, 9 (3), 233-248.
662 McNinch, J.E., 2004. Geological control in the nearshore: shore-oblique sandbards and shoreline
663 erosional hotspots, Mid-Atlantic Bight, USA. Marine Geology 211, 121-141.
664 Mentaschi, L., Vousdoukas, M.I., Pekel, J.-F., Voukouvalas, E. and Feyen, L., 2018. Global long-term
665 observations of coastal erosion and accretion. Scientific Reports, 8(1): 12876.
666 Newton, A.R., Shone, R.W., Booth, P.W.K., 2006. The Cape Fold Belt. In: Johnson, M. R., Annhauser,
667 C. R. and Thomas, R. J. (Eds.), The Geology of South Africa. Geological Society of South
668 Africa, Johannesburg/Council for Geoscience Pretoria, 521-531.
669 Perez, J., Menendez, M., Losada, I., 2017. GOW2: a global wave hindcast for coastal applications.
670 Coastal Engineering, 124, 1-11.

671 Senechal, N., Coco, G., Castelle, B., Marieu, V., 2015. Storm impact on the seasonal shoreline dynamics
672 of a meso- to macrotidal open sandy beach (Biscarrosse, France). Geomorphology, 228, 448-
673 461.
674 Senechal, N, Alegria-Arzaburu, A.R., 2020. Seasonal imprint on beach morphodynamics. In Jackson,
675 D.W.T. and Short, A.D. (Eds), Sandy Beach Morphodynamics. Elsevier, pp. 461-486.
676 Stive, M.J.F., Aarninkhof, S.G.J., Hamm, L., Hanson, H., Larson, M.,Wijnberg, K.M., Nicholls,
677 R.J., Capobianco, M., 2002. Variability of shore and shoreline evolution. Coast. Eng. 47
678 (2), 211–235. https://doi.org/10.1016/S0378-3839(02)00126-6.
679 Smith AM, Guastella LA, Botes ZA, Bundy SC, Mather AA. 2014. Forecasting cyclic coastal erosion
680 on a multi-annual to multidecadal scale: southeast African coast. Estuarine, Coastal and Shelf
681 Science 150(part A): 86–91.
682 South African Navy, 2017. South African Tide Charts. Published by the Hydrographer of the South
683 African Navy. 8 pp. ISBN 978-0-9869717-8-5
684 Storey, J., Scaramuzza, P., Schmidt, G., Barsi, J., 2005. Landsat 7 scan line corrector-off gap-filled
685 product development. In Proceedings of the Pecora 16 Conference on Global Priorities
686 in Land Remote Sensing, Sioux Falls, SD, USA, 23–27 October 2005; 13 p.
687 Storlazzi, C., Elias, E., Field, M., Presto, M., 2010. Numerical modelling of the impact of sea-level rise
688 on fringing coral reef hydrodynamics and sediment transport. Coral Reefs 83 – 96.
689 Thieler et al., 1995 Geology of the Wrightsville Beach, North Carolina shoreface; implications for the
690 concept of shoreface profile of equilibrium. Mar. Geol., 126, pp. 271-287
691 Thieler, E.R., Himmelstoss, E.A., Zichichi, J.L., Ergul, A, 2009. Digital Shoreline Analysis System
692 (DSAS) version 4.3 — An ArcGIS extension for calculating shoreline change: U.S. Geological
693 Survey Open-File Report 2008-1278.
694 Thom, B., 2020. Future challenges in beach management as contested spaces . In Jackson, D.W.T. and
695 Short, A.D. (Eds), Sandy Beach Morphodynamics. Elsevier, pp. 711-731.
696 Thornton, E.B., MacMahan, J., Sallenger, A.H., 2007. Rip currents, mega-cusps and eroding dunes.
697 Marine Geology, 240, 151-167.

698 Umeda, S., Yuhi, M., Karunarathna, H., 2018. Seasonal to decadal variability of shoreline position on
699 a multiple sandbar beach. Journal of Coastal Research, Special Issue 85. Proceedings of the 15th
700 International Coastal Symposium 261 – 265.
701 Velegrakis, A.F., Trygonis, V., Chatzipavlis, A.E., Karambas, T. V., Vousdoukas, M.I., Ghionis, G.,
702 Monioudi, I.N., Hasiotis, Th. Andreadis, O., Psarros, F., 2016. Shoreline variability of an urban
703 beach fronted by a beachrock reef from video imagery. Natural Hazards 201 – 222.
704 Vousdoukas, M.I., Velegrakis, A.F. Plomaritis, T. A., 2007. Beachrock occurrence, characteristics,
705 formation mechanisms and impacts. Earth-Science Review, 85, 23 – 46.
706 Vousdoukas, M.I., Velegrakis, A.F., Karambas, T.V., 2009. Morphology and sedimentology of a
707 microtidal beach with beachrocks: Vatera, Lesbos, NE Mediterranean. Continental Shelf
708 Research, 29, 1937 – 1947.
709 Vousdoukas, M.I., Ranasinghe, R., Mentaschi, L. Plomaritis, T. O., Athanasiou, P., Luijendijk A., and
710 Feyen, L. Sandy coastlines under threat of erosion 2020. *Nat. Clim. Chang.* **10,** 260–263.
711 https://doi.org/10.1038/s41558-020-0697-0
712 Vousdoukas, M.I., Clarke, J., Ranasinghe, R. *et al.* African heritage sites threatened as sea-level rise
713 accelerates. *Nat. Clim. Chang.* (2022). https://doi.org/10.1038/s41558-022-01280-1
714 Walton, T.L., Sensabaugh, W., 1979. Seawall Design on the Open Coast, Florida Sea Grant College
715 Rpt No. 29, Florida.
716 Wu, X. *et al*., 2021. Quantification of the Uncertainty Caused by Geometric Registration Errors in
717 Multiscale Validation of Satellite Product. *IEEE Geoscience and Remote Sensing Letters*, 19,
718 1-5. doi: 10.1109/LGRS.2021.3099833.
719
720
721